Bulletin of the Seismological Society of America, Vol. 87, No. 3, pp. 731–744, June 1997

Near-Surface Attenuation and Site Effects from Comparison of Surface and Deep Borehole Recordings

by Rachel E. Abercrombie*

Abstract Near-surface attenuation and site effects are investigated using the seismograms of 17 local earthquakes recorded at depths of 0, 0.3, 1.5, 2.5, and 2.9 km in the Cajon Pass borehole, southern California. The borehole penetrates 500 m of Miocene sandstone and then crystalline, granitic basement rock. Previous estimates of site response have been limited to shallower holes, where the surface reflection interferes with the upgoing direct wave, and the deepest sensor is not below the severe near-surface effects, in bedrock. Spectral ratios of the direct P and S waves for each earthquake between the different recording levels are well modeled with frequency-independent Q and amplification. At the borehole, $Q_P \sim 27 \pm 8$, and $Q_S \sim 21 \pm 7$ in the upper 2.9 km, increasing from $Q_P \sim 26$ and $Q_S \sim 15$ in the upper 300 m to $Q_P \sim 133$ and $Q_S \sim 47$ between 1.5 and 3 km. One event was also recorded at a surface granite site, less than 1.5 km from the wellhead. Comparison of the 2.9-km recording with that at this granite site gives $Q_P \sim 50$ and $Q_S \sim 23$. The similarity of these values with those of previous studies at a wide range of sites suggests that Q is very low in the near surface, independent of rock type. Near-surface amplification appears considerably more site dependent. At the wellhead, the amplifications at 1 Hz of the direct P and S waves are 12 ± 7 and 13 ± 7, respectively. These values include the free-surface effect and are in reasonable agreement with the impedance contrast from the borehole logs. At the granite site, amplification of both P and S waves is less than four; direct-wave amplification at the wellhead is therefore at least three times that of the granite site. The spectra of the direct and coda waves of the one earthquake recorded at both the wellhead and granite sites are compared with the corresponding 2.9-km recording. Coda-wave amplification is in good agreement with the direct wave at the rock site, but at the borehole, the coda-wave amplification factor overestimates the direct-wave amplification by a factor of 3.

Introduction

The distortion of seismic waves, including attenuation, amplification and scattering, in the near-surface rocks is commonly referred to as the site effect. The importance of understanding site effects has become increasingly clear, both in predicting ground motions in future large earthquakes and in investigations of the earthquake source itself. The patterns of peak ground shaking and resulting damage in recent large earthquakes (e.g., Michoacan, 1985, Loma Prieta, 1989, Northridge, 1994, and Kobe, 1995) are clearly linked to the underlying site conditions, with sediments amplifying waves by as much as 10 and also significantly prolonging the duration of shaking (for example, in Mexico City, Celebi *et al.,* 1987). Information about site conditions is clearly invaluable in assessing seismic risk, improving building codes, and assessing the degree of retrofitting needed for existing structures. Also, studies of the earthquake source, to determine rupture dimension, stress drop, and other source parameters, must correctly account for the site effect, along with other path effects, or else the parameters calculated will be erroneous (Abercrombie and Leary, 1993; Abercrombie, 1995a; Zeng and Anderson, 1996).

Typically, site-effect studies compare the sites of interest, usually sedimentary, to a bedrock reference site, the assumption being that the bedrock recording is the same as the waveform incident at the base of the sediments (or complex near-surface structure) at the site of interest. Many such studies have been performed using direct S waves (e.g., Field *et al.,* 1992), coda waves (e.g., Phillips and Aki, 1986), and whole seismograms (e.g., Borchedt, 1970). Differences between sites can be identified and site resonances picked out

*Present address: Institute of Geological and Nuclear Sciences, 32 Salamanca Road, P.O. Box 1320, Wellington, New Zealand.

reliably when a large number of recordings are available and suitably averaged (Field and Jacob, 1995). None of these methods, however, are able to determine the absolute amount of amplification or attenuation at the sites, as the real difference between the bedrock reference recording and the waveform as it left the source (including any reference site "site effect") is not known. This problem is clearly of particular importance in studies of the earthquake source. In order to address this problem, a large number of borehole seismometers have been deployed, typically at depths of a few hundred meters. Comparison of the recordings at the wellhead and downhole allows estimation of the site effect, and the recordings downhole can be used for source studies, as they are uncontaminated by travel through the surface layers. Studies such as those by Seale and Archuleta (1989) near Mammoth Lakes, Blakeslee and Malin (1991) at Parkfield, Aster and Shearer (1991) at Anza, and Archuleta *et al.* (1992) at Garner Valley, California, have all found very low values of Q (~5 to 10) in the upper few tens to hundreds of meters. Reliable determination of the site effect has, however, been limited by the interference of the surface reflection with the upgoing direct wave at the borehole seismometers (Shearer and Orcutt, 1987). Also, as noted by Blakeslee and Malin (1991), a few hundred meters is not deep enough to get below the entire site effect, and thus, the seismograms are still contaminated by local site conditions and the surface reflection. Hauksson *et al.* (1987) compare recordings of a single earthquake made at depths up to 1500 m to determine Q_S ~25 (420 to 1500 m). The borehole location, however, is in a part of the Los Angeles basin where the sediments are about 4 km deep (Yerkes *et al.*, 1965), and so again the whole effect of the sediments is not observed.

Deeper borehole recordings in bedrock would thus seem appropriate to this problem, and here the site effects around the Cajon Pass borehole, southern California, are investigated by comparing earthquake seismograms recorded at the surface and at 0.3, 1.5, 2.5, and 2.9 km depth (Fig. 1). In particular, I concentrate on the attenuation and amplification of the direct P and S waves as they travel through the upper 3 km. These parameters are of great importance to earthquake source studies, and their effect has been controversial (Archuleta *et al.*, 1982; Anderson, 1986). Abercrombie and Leary (1993) and Abercrombie (1995a) have shown that propagation through the near surface has a significant effect on the seismograms of small and moderate earthquakes. Here these effects are considered in more detail and quantified. Comparison of the direct-wave amplification and attenuation estimates with the borehole density and velocity logs also allows evaluation of how well the effects of the near surface on the direct waves can be estimated from such site-specific geophysical information.

Calculation of the spectral ratio between the shallow or surface recordings and the deeper one is the most straightforward method of investigating the amplification and attenuation on the path in between. This method was used successfully by Hauksson *et al.* (1987), Aster and Shearer (1991), and others and is adopted here. The underlying assumption is that the deeper recording can be considered on the ray path between the source and the upper receiver. For this reason, only earthquakes that occur close to, but deeper than, the borehole can be used.

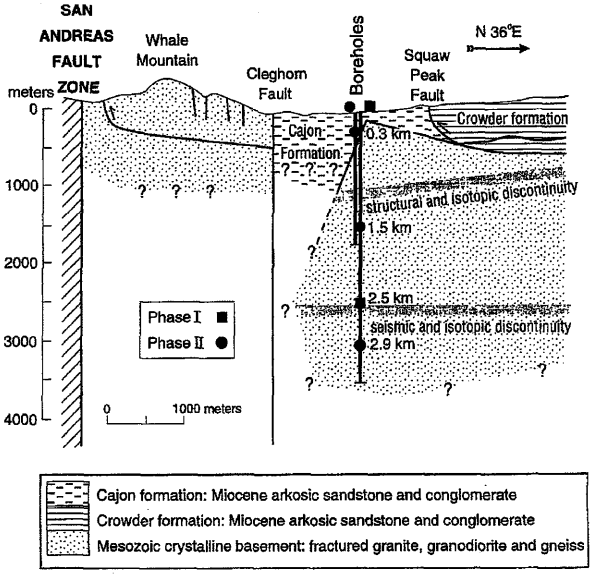

Figure 1. Vertical cross section perpendicular to the San Andreas fault (after Silver and James, 1988a,b) showing the depths of the instruments deployed at Cajon Pass during phases I and II. The 1.5-, 2.5-, and 2.9-km-deep instruments were installed in the Cajon Pass scientific drillhole. The 0.3-km-deep instrument was installed in the neighboring, 1795-m-deep "Arkoma" hole, 50 m away.

Geological Setting and Instrumentation of the Cajon Pass Borehole

The Cajon Pass drillhole is located about 4 km northeast of the San Andreas fault, in southern California, between the rapidly rising San Gabriel and San Bernadino Mountains that bound the Los Angeles basin (Figs. 1 and 2). The hole passes through 500 m of Miocene, arkosic sandstone (the Cajon Formation, Meisling and Weldon, 1989), and then into Mesozoic crystalline bedrock to a total depth of 3.5 km (Silver and James, 1988a). The interface between the sediments and the basement is a steeply dipping (>70°) faulted contact (Silver and James, 1988b). This site is of interest as it allows investigation of the effects of a small sedimentary basin and of crystalline basement rock at shallow depths. A seismometer was also installed for part of the duration of the experiment on intact granite, outcropping less than 1.5 km from the wellhead. Comparison of the deep recordings with those at the granite site allows estimation of the site effect of a typical reference site.

The recording at Cajon Pass was carried out in two

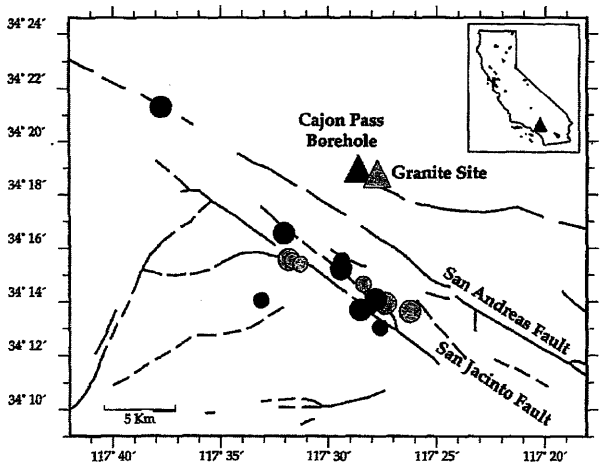

Figure 2. Map showing the Cajon Pass borehole (black triangle), the nearby granite site (gray triangle), local faults, and the epicenters of earthquakes used in this study. Gray circles are events recorded during phase I, and black circles are those recorded during phase II. The inset shows the location of the borehole (triangle) in the state of California.

phases: phase I, from August 1991 to August 1993 at the wellhead and at 2.5 km depth, and phase II, from November 1993 to December 1994 at the wellhead and at 0.3, 1.5, and 2.9 km depth. Three-component geophones were deployed at all levels, but logistical constraints, principally the high operating temperatures (>100°C) and pressures at the deeper levels [see Manov *et al.* (1996) for further details], lead to a variety of instruments being used. All of the geophones were calibrated *in situ* using the technique of Rodgers *et al.* (1995) to enable accurate correction for instrument response. At the surface (both at the wellhead and at the temporary granite site), 2-Hz L22-D sensors were used; at 300 m depth, 4.5-Hz L1-B geophones; and at the three deeper levels, 10-Hz L-15LA high-temperature geophones. All of the sensors were recorded using RefTek recorders, with the following sample rates: 250 samples/sec at the surface, 500 samples/sec at 300 m and 2.5 km, and 1000 samples/sec at 1.5 and 2.9 km. Good coupling to the ground of the surface instruments was obtained using plaster of paris and by burying them. The borehole seismometers all had to be retrievable, however, and so were clamped into the hole. The borehole instrument packages and clamping design are described in detail by Manov *et al.* (1996). Clamping the instruments could not completely eliminate some resonance of the seismometer package within the borehole, at 45 to 55 Hz on the horizontal components, principally the one perpendicular to the clamping arm (Manov *et al.*, 1996; Leary *et al.*, 1990). This resonance was of small amplitude for the events considered here and was found to have a negligible effect on the spectral ratios. Comparison of ratios using all three downhole components with those using only the vertical (unaffected by the resonance) found no systematic differences in slope.

Phase I: 0 and 2.5 km

Six (M_L 1.3 to 2.8) earthquakes were recorded during phase I that were close to the borehole (epicentral distance <10 km, Fig. 2) and large enough to have good signal-to-noise ratios at the surface instrument. Lower noise levels at the downhole instruments ensure higher signal-to-noise ratios than at the surface, despite significant amplification of surface waveforms. Hypocentral parameters of the earthquakes used in both phase I and II of this study are listed in Table 1. An example of the three-component recordings of one of the events is shown in Figures 3a and 3b. All of the seismograms and spectra used in this analysis are corrected for instrument response. The 0.5-sec time windows used for calculating the spectra are also shown. They start 0.03 sec prior to the picked phase arrival to allow for a 5% cosine taper. The choice of time window is typically a compromise between isolating arrivals of relatively short time duration, and stability and resolution of lower frequencies. In this study, the aim is to investigate the effect of the near-surface rocks on the direct P and S waves, so short time windows are preferred. Source durations of earthquakes of $M_L \leqq 2.8$ are typically $\leqq 0.1$ sec (Abercrombie, 1995a). The lowest signal frequencies typically observed for earthquakes of the magnitude included in this study, recorded at Cajon Pass, are 2 to 3 Hz; the low noise level downhole enables signals to be retrieved from below the geophone corner frequency (see also Abercrombie, 1995a). A 0.5-sec window was selected as the shortest able to resolve these frequencies. Such a window length is considerably longer than the downhole and surface pulses (Figs. 3c and 3d) but limits the surface coda included (Fig. 3a) and also excludes the surface reflection at the 2.5-km site. Interference between the upgoing wave and the surface reflection at the borehole site results in holes in the frequency amplitude spectrum, making it difficult to interpret spectral ratios (Shearer and Orcutt, 1987). This effect is decreased by the severe attenuation of the surface reflection as it travels through the near-surface rocks, but in this study, it is preferred to avoid it completely. The time delays between the P and S arrivals at the borehole and surface instruments are typically about 0.5 and 1 sec (see Table 2), respectively, so that the surface reflections should be approximately 1 and 2 sec after the direct wave at the 2.5-km site. In order to check that the results were not strongly dependent on the choice of window length, the spectral analysis was also performed using 1 sec windows. The resulting values of Q and amplification were similar to, and well within the error limits of, those using 0.5-sec windows. For these reasons, 0.5-sec time windows are used to calculate all the spectra used in the following analysis.

The spectra of the event shown in Figure 3 are plotted in Figures 4a and 4b for P and S waves, respectively. The dominant effects of propagation through the near-surface

Table 1

Hypocentral parameters from the Southern California Seismic Network (SCSN) of the 17 earthquakes considered in this study. Values of hypocentral distance and depth marked with an asterisk are calculated from the *P* and *S* arrival times and the incoming angle at the deepest recording level. An "X" indicates that the earthquake was recorded at that depth. *Azi* is the incoming azimuth.

ID	Date (Yr/Mo/Dy)	M_L	Lat. (34° min)	Long. (−117° min)	Depth (km)	Hypocentral Distance (km)	Azi (°)	Recording Depth (km)					Angle of Incidence (°)		
								0	0.3	1.5	2.5	2.9	1.5	2.5	2.9
I1	92/4/22	2.8	13.64	26.25	13	15	159	X			X			42	
I2	92/5/13	1.7	14.65	28.39	12	13	177	X			X			38	
I3	92/5/26	2.0	13.93	27.37	12	14	168	X			X			33	
I4	92/6/21	2.5	15.56	31.87	7	10	219	X			X			46	
I5	92/6/21	1.9	15.52	31.71	8	10	217	X			X			42	
I6	92/6/22	1.3	15.39	31.11	10	12	213	X			X			46	
II1	93/12/1	0	—	—	11*	9*	240*	X	X	X		X	11		23
II2	94/1/6	0	—	—	5*	7*	230*	X	X	X		X	43		65
II3	94/1/23	1.3	13.03	27.62	13	16	172	X	X	X			39		
II4	94/2/25	2.1	16.54	32.08	11	12	231	X	X	X		X	19		33
II5	94/4/17	1.6	14.04	33.15	10	14	218			X		X	38		54
II6	94/5/19	2.1	13.69	28.54	8	12	175	X	X	X		X	34		56
II7	94/5/19	1.6	13.80	28.13	9	12	175	X	X	X		X	33		58
II8	94/7/10	1.5	15.52	29.41	14	14	191	X	X	X			11		
II9	94/8/22	2.3	21.30	37.78	10	17	288	X	X	X		X	30		52
II10	94/9/21	2.3	14.09	27.82	12	13	172	X	X	X		X	19		32
II11	94/9/23	2.4	15.22	29.43	12	13	188			X		X	20		25

rocks are amplification below about 10 Hz and attenuation at higher frequencies. These effects are responsible for the pulse broadening seen in Figures 3c and 3d. The spectral ratios are calculated by dividing the surface spectra by those recorded in the borehole, after correcting for the different instrument responses. No smoothing is performed, and only the frequencies where the signal is at least three times the noise level at both instruments are used. In the case of *P* waves, the noise spectrum is that of the 0.5-sec time window preceding the *P* arrival. The noise spectrum for the *S* waves is calculated from the last 0.5 sec of the *P*-wave coda. Use of the pre-event noise level to identify the signal bandwidth of the *S* wave leads to the inclusion of high-frequency *P*-wave coda in the ratio and underestimation of the *S*-wave attenuation. In order to account for the different incidence angles at the instruments, and different backazimuths of the earthquakes, the spectra are calculated as follows. The *P*-wave surface spectrum is calculated from the vertical component only, and the *S*-wave spectrum is the vector sum of the spectra of the two horizontals as the incidence is vertical. At 2.5 km, however, the incoming rays have not been refracted to vertical incidence (notice the significant amplitudes of the *S* wave on the vertical component and the *P* wave on the horizontals in Fig. 3b). The incidence angles are obtained by rotating the three components of the first *P*-wave velocity pulse to obtain the direction of maximum *P*-wave amplitude, associated with the incoming direction of the wave. They are included in Table 1. This calculation is accurate to within ± about 3°, and the resulting directions are in excellent agreement with those calculated from the SCSN locations of the events (Abercrombie, 1995b). The *P*- and *S*-wave spectra at 2.5 km are, therefore, both calculated from the vector sum of the amplitude spectra of all three components. In this manner, the amplification values obtained in this study have been corrected for geometrical effects resulting from the difference in incidence angle at the different recording depths.

The spectral ratios of the event in Figure 3 are shown in Figures 4c and 4d. The spectral ratios are calculated for each individual event, and then the mean ratios of all six events are determined (Fig. 5). The linear nature of the ratios on the log-linear plots implies that they will be well matched by an exponential attenuation model, with both amplification and Q independent of frequency (f):

$$A(f) = A_0 e^{-\pi f t^*}, \quad (1)$$

where A is the ratio amplitude, A_0 is the amplification at 0 Hz, and t^* is the travel time between the two recordings divided by Q. Such a model has been used successfully in a number of previous studies, for example, Hauksson *et al.* (1987) and Aster and Shearer (1991). There has been some suggestion that Q is dependent on frequency in at least part of the frequency range considered here (Jin *et al.*, 1994; Leary and Abercrombie, 1994). The linear nature of the spectral ratios, however, shows that any frequency dependence of Q in the near-surface rocks must be small or be matched by complementary frequency dependence of amplification. The latter seems unlikely, suggesting that Q is predominantly frequency independent in this bandwidth (~3 to 100 Hz) and depth interval. The important observation is that the relation in equation (1) is able to match the data well and so can be considered a good description of the effects of the near-surface rocks for seismic hazard and earthquake

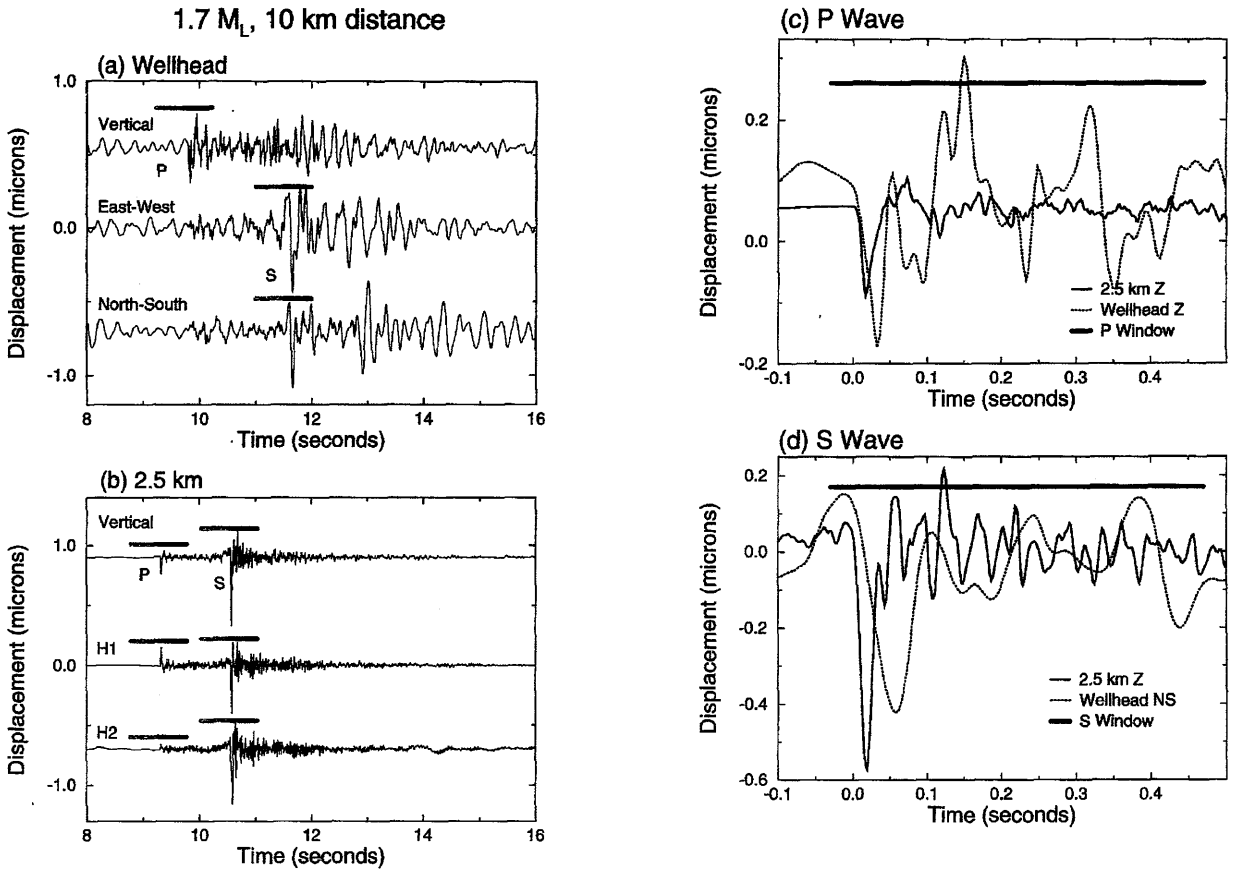

Figure 3. Comparison of seismograms of event I2 recorded at 2.5 km depth and at the wellhead. Three-component seismograms, corrected for instrument response and flat to displacement between 1 and 200 Hz at (a) the wellhead and (b) 2.5 km. Note that phaseless filtering is used. The horizontal black bars indicate the time windows used to calculate the *P* and *S* spectra for analysis (starting 0.03 sec prior to the picked arrival time), and the gray bars, the noise windows used. Enlargement of the (c) *P*-wave and (d) *S*-wave time windows from (a) and (b) shows the coherency of pulse shapes between the borehole and surface sites. The *P* and *S* waves are aligned with their arrival times at 0. Notice the broadening of the *S* pulse (and, to a lesser extent, the *P* pulse) at the surface compared to downhole. For the *S* wave, the vertical-component downhole is compared with the N–S horizontal at the surface. As the earthquake is almost due south of the borehole, this approximates to comparing the radial component of the *S* wave at both sites.

source parameter studies. The t^* and A_0 for each individual spectral ratio and for the average ratios shown in Figure 5 are determined from least-squares fitting with equation (1), which is a linear relationship between log amplitude and linear frequency. These fits are shown in Figures 4c, 4d, and 5. The resulting estimates of t^* and Q for each earthquake are given in Table 2 and the mean values in Table 3. The individual earthquake values provide an indication of the variation produced by the complex near-surface structure at the borehole (Fig. 1), whereas the parameters calculated from the mean ratios are an additional estimate of the average near-surface properties. In Tables 2 and 3, the resulting amplification at 1 Hz (calculated from A_0 using t^* and equation 1) is quoted, rather than A_0. These values are preferred as they are closer to the frequency range of the data (typically $\geqq$3 Hz) and also to the frequencies of most interest in site response. Although the spectral ratios are relatively linear in the frequency range observed here, this may not be the case at lower frequencies, and so A_0 may not be a good estimate of the amplification at 0 Hz. Also, note that equation (1) does not contain a separate term for the effect of reflection at the free surface. When the upper site considered is at the surface, as is the case for all the ratios in phase I, A_0 and A_1 include the free-surface effect (often taken as a factor of 2).

Table 2

Travel time between the two depths (tP and tS), t^*, Q (Q_P for P waves and Q_S for S waves), the frequency range over which the spectral ratios are modeled (Pf and Sf range), and amplification values (A_P for P waves and A_S for S waves) for all 17 earthquakes. The amplification values are those at 1 Hz calculated from A_0 and t^* using equation (1).

(a) Phase I (0 to 2.5 km)

ID	tP (s)	tS (s)	t^*P ($\times 10^{-3}$ sec)	Pf Range (Hz)	t^*S ($\times 10^{-3}$ sec)	Sf Range (Hz)	Q_P	Q_S	A_P (1 Hz)	A_S (1 Hz)
I1	0.525	1.085	15.7	8–104	49.0	3–21	32	22	4.4	11
I2	0.489	1.017	13.9	4–104	61.4	3–21	34	17	6.6	17
I3	0.497	0.995	14.7	8–82	41.9	3–29	34	24	8.6	8.2
I4	0.485	1.015	23.6	7–76	65.6	6–50	21	16	22	9.6
I5	0.477	1.017	22.5	5–82	58.7	4–21	21	17	15	7.8
I6	0.475	1.003	22.5	4–77	67.6	5–21	21	15	15	21
Mean	0.49	1.02	17.1	—	47.0	—	29	22	8.2	9.5

(b) Phase II—travel times: An asterisk indicates that the event occurred when no clock was operating and that the times are calculated from the mean of the times recorded for other events using the incidence angles to correct for geometry.

	tP (sec)			tS (sec)		
ID	2.9–1.5 km	1.5–0.3 km	0.3–0 km	2.9–1.5 km	1.5–0.3 km	0.3–0 km
II1	0.204	0.232	0.160	0.338	0.454	0.446
II2	0.110*	0.200*	0.168*	0.192*	0.414*	0.457*
II3	—	0.191	0.187	—	0.418	0.408
II4	0.184*	0.220*	0.168*	0.322*	0.455*	0.457*
II5	0.115*	—	—	0.200*	—	—
II6	0.120*	0.215*	0.168*	0.210*	0.445*	0.457*
II7	0.120*	0.215*	0.168*	0.210*	0.445*	0.457*
II8	—	0.226	0.168	—	0.444	0.441
II9	0.127	0.216	0.165	0.236	0.469	0.418
II10	0.184	0.212	0.159	0.328	0.448	0.399
II11	0.198	—	—	0.341	—	—

(*continued*)

Phase II: 0, 0.3, 1.5, and 2.9 km, and Granite Site

During phase II, 11 earthquakes ($M_L \leqq 2.4$) were recorded at two or more different levels in the borehole and are used in this study (Table 1, Fig. 2). Two of these were too small to trigger the SCSN (complete above $\sim M_L$ 1.8 in this area) and so are not plotted in Figure 2. Only the most northwesterly event (II9), on the San Andreas fault, was recorded at the granite site, and it was also recorded at all levels in the borehole and so is used as the example. Figure 6a shows the seismograms of this event recorded at the four-level borehole array and at the granite site. The spectra are calculated as described for phase I, with the 300-m and granite sites being treated like the wellhead site, assuming that the incoming waves are refracted to the vertical. This assumption is borne out by the relative amplitudes of the P and S waves on the three components for the events used. For example, note the low amplitude of the S wave on the vertical component at the 300-m, wellhead, and granite sites in Figure 6a. The 1.5- and 2.9-km sites are treated like the 2.5-km level because the incoming waves have not been refracted to the vertical. Again, 0.5-sec time windows are used at all levels for both the P and S waves. The spectra are shown in Figure 6b. The S-wave spectra show clearly the attenuation of the high frequencies at the 300-m and surface sites. It is also interesting to note that whereas the wellhead site experiences considerable amplification, little is seen at the granite site. These observations are confirmed by the mean spectral ratios plotted in Figure 7. The values of amplification, t^*, and Q obtained by modeling the mean and individual spectral ratios using equation (1) are shown in Tables 2 and 3.

Results and Discussion

The near-surface attenuation, amplification, and velocity parameters obtained for the Cajon Pass site are summarized in Table 3. The Q and velocity estimates below 2.5 km are those of Abercrombie (1995a,b) obtained by modeling the source spectra of over a hundred earthquakes recorded at 2.5 km. A frequency-independent Q of 1000 fits both P and S waves well. The velocity values are typical of such crustal depths in this area (e.g., the velocity structure inversion by Magistrale *et al.*, 1992) and are in good agreement with the angles of incidence and the locations of the earthquakes by the SCSN. When the Q values obtained for the upper 3 km are compared with these values for greater depths, it is clear that most of the attenuation of earthquake seismic waves is occurring in the near surface. For example,

Table 2
Continued

(c) Phase II; *P*- and *S*-wave t^* ($\times 10^{-3}$ sec), and the frequency ranges used in the spectral ratio modeling (*fP* and *fS*, Hz). Ratios are not modeled when either recording of the pair does not have sufficient signal to noise (e.g., II1 *S* waves), or when a recording is clipped (#).

	2.9–0 km				2.9–1.5 km				1.5–0.3 km				0.3–0 km				2.9–0.3 km			
ID	t^*P	*fP*	t^*S	*fS*	t^*P	*fP*	t^*S	*fS*	t^*P	*fP*	t^*S	*fS*	t^*P	*fP*	t^*S	*fS*	t^*P	*fP*	t^*S	*fS*
II1	—	—	—	—	1.86	6–176	—	—	4.50	8–54	—	—	—	—	—	—	7.39	8–54	—	—
II2	23.7	13–39	69.1	7–19	4.47	13–144	11.7	7–37	7.54	9–44	32.1	6–21	13.9	10–39	13.6	7–19	14.0	13–44	51.9	7–21
II3	—	—	—	—	—	—	—	—	3.95	10–117	15.0	6–23	—	—	30.2	9–19	—	—	—	—
II4	23.2	15–59	38.0	4–18	1.91	8–249	8.79	5–57	9.63	8–54	20.8	5–26	8.38	15–54	19.0	2–18	14.2	5–54	15.8	4–26
II5	—	—	—	—	2.26	8–173	4.02	5–32	—	—	—	—	—	—	—	—	—	—	—	—
II6	18.8	15–61	—	—	1.29	6–215	8.14	5–35	6.55	5–54	13.6	5–29	9.85	15–54	—	—	11.4	6–54	20.6	5–29
II7	20.3	14–68	—	—	1.44	7–208	5.70	6–39	4.60	6–59	16.0	5–29	5.80	14–59	—	—	11.0	7–59	21.3	6–29
II8	—	—	—	—	—	—	—	—	6.16	7–117	18.0	6–26	3.28	16–63	—	—	—	—	—	—
II9	23.3	6–47	63.4	4–16	2.82	5–98	1.82	4–49	8.26	5–54	23.4	4–25	13.1	6–47	65.6	4–16	10.8	5–54	26.9	4–25
II10	12.0	8–80	33.2	5–20	1.10	5–254	4.86	5–82	—	—	—	—	—	—	—	—	—	—	—	—
II11	—	—	—	—	0.69	6–267	#	#	—	—	—	—	—	—	—	—	—	—	—	—

(d) Phase II: *P*- and *S*-wave *Q* and amplification (1 Hz) values.

	2.9–0 km				2.9–1.5 km				1.5–0.3 km				0.3–0 km				2.9–0.3 km			
ID	Q_P	Q_S	A_P	A_S	Q_P	Q_S	A_P	A_S	Q_P	Q_S	A_P	A_S	Q_P	Q_S	A_P	A_S	Q_P	Q_S	A_P	A_S
II1	—	—	—	—	110	—	0.9	—	52	—	0.8	—	—	—	—	—	59	—	0.7	—
II2	20	15	17	29	25	16	1.0	1.1	27	32	2.2	3.1	12	34	8.7	18	22	12	2.9	5.2
II3	—	—	—	—	—	—	—	—	48	28	0.6	1.5	—	14	—	13	—	—	—	—
II4	25	32	28	5.0	96	37	0.9	1.4	23	22	0.6	0.6	20	24	30	6.3	28	49	1.0	0.5
II5	—	—	—	—	51	50	0.6	0.7	—	—	—	—	—	—	—	—	—	—	—	—
II6	27	—	7.5	—	93	26	0.6	1.5	33	33	0.9	1.6	17	—	9.8	—	29	32	0.9	2.3
II7	25	—	8.5	—	83	37	0.6	1.5	47	28	0.8	2.0	29	—	6.2	—	30	31	0.9	3.1
II8	—	—	—	—	—	—	—	—	37	25	1.3	2.1	51	—	5.9	—	—	—	—	—
II9	22	18	15	9.7	45	130	0.9	0.7	26	20	1.7	2.1	13	6.4	11	49	32	26	1.5	1.6
II10	46	35	3.0	8.7	167	67	0.5	1.0	—	—	—	—	—	—	—	—	—	—	—	—
II11	—	—	—	—	287	#	0.4	#	—	—	—	—	—	—	—	—	—	—	—	—

(e) Phase II: Results for granite site relative to 2.9 km depth, for event II9.

tP (sec)	*tS* (sec)	t^*P($\times 10^{-3}$ sec)	*P f* Range (Hz)	t^*S($\times 10^{-3}$ sec)	*S f* Range (Hz)	Q_P	Q_S	A_P (1 Hz)	A_S (1 Hz)
0.586	1.126	11.8	6–55	49.1	6–25	50	23	1.2	3.6

for an earthquake recorded at the wellhead with a hypocentral distance of up to 15 km, over 90% of the attenuation is occurring in the upper 3 km and 50% in the upper 300 m. This latter proportion is the same as that estimated by Aster and Shearer (1991) at Anza on the southern California batholith. This study therefore confirms that site effects must be taken into account when studying earthquake source parameters. Even at a good granite site, near-surface attenuation causes a decrease in amplitude at 25 Hz with respect to 1 Hz of factors of about 3 and 40 for *P* and *S* waves, respectively.

The *Q* values obtained in this study for the upper 300 m are in good agreement with previous borehole studies of near-surface attenuation in California, which are summarized in Table 4. These studies, combined with the present one, indicate that *Q* decreases to very low values in the near surface, regardless of rock type. In the present study, and previous ones where two or more borehole depths were instrumented, *Q* can be seen to increase rapidly with depth. It is therefore probable that in each depth interval, the average *Q* value is dominated by very high attenuation in the upper part, and the deeper part may be considerably less attenuating. At Anza, however, low *Q* values extend below 150 m (Aster and Shearer, 1991), and at Oroville, below 300 m (Malin *et al.* 1988). In the present study, low *Q* values are observed to extend below 1.5 km. As previously noted by Blakeslee and Malin (1991), studies of small earthquake sources using shallow borehole recordings, even in crystalline bedrock, cannot assume reliably that all significant near-surface attenuation has been avoided.

The similarity of the *Q* estimates in this study and previous borehole studies in California (Table 4) in a range of rock types suggests some other factor is principally responsible for the rapidly increasing attenuation toward the sur-

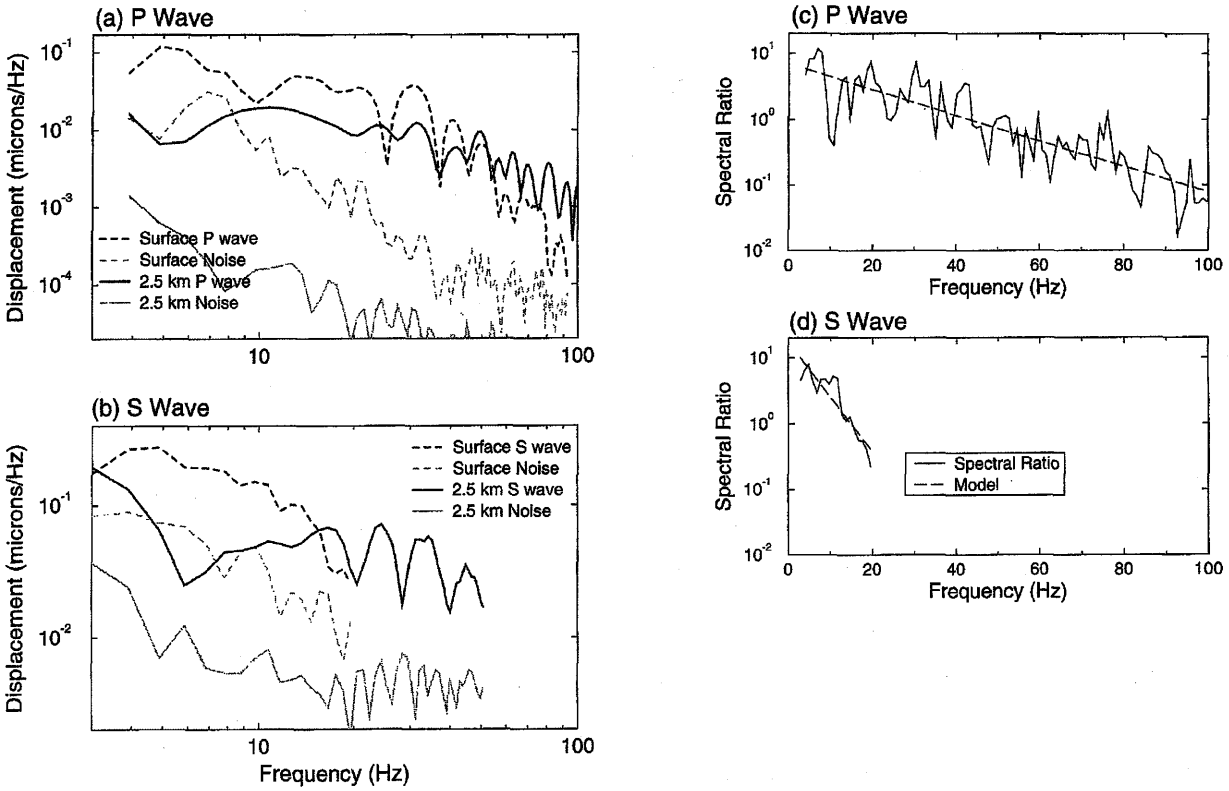

Figure 4. Comparison of spectra of event I2 recorded at 2.5 km depth and at the wellhead. Displacement amplitude spectra of (a) *P* and (b) *S* waves (black) and the noise level (gray). Only the bandwidth corresponding to the signal used in the spectral ratios is shown. Notice that at low frequencies the wellhead recordings are amplified with respect to the deep recordings, but at higher frequencies, energy present at 2.5 km has been attenuated out before it reaches the surface. Spectral ratios of the wellhead divided by the 2.5 km spectra of (c) *P* waves and (d) *S* waves. The best fits using equation (1) are shown as dashed lines, and the parameters are given in Table 2.

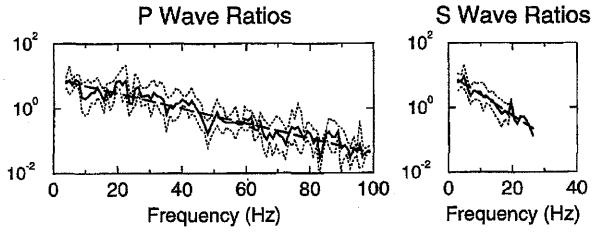

Figure 5. The mean spectral ratios (0/2.5 km) of all six earthquakes recorded in phase I (solid lines). Each event is included over the frequency ranges given in Table 2. The dotted lines are one standard deviation, and the dashed lines are the best fits using equation (1) (the parameters are given in Table 2). Note that on the log-linear plots the spectral ratios are well modeled by a straight line. Both plots are at the same scale.

face. Laboratory studies of attenuation find that both Q_P and Q_S increase rapidly with increasing pressure up to about 500 to 1000 bars (equivalent to about 1.5 to 4 km depth at Cajon Pass) and then level off (Johnston *et al.*, 1979). This pressure dependence of attenuation has been interpreted as resulting from the closure of cracks in the rocks with increasing pressure. Johnston *et al.* (1979) find that at the pressures considered in this study, friction at cracks is the most probable dominant mechanism of intrinsic attenuation. Fractures are major scatterers of seismic energy, and so scattering attenuation should also decrease with increasing pressure, as the fractures are closed. Mori and Frankel (1991) observed a significant decrease in scattering attenuation below about 5 km in southern California. Laboratory and field results thus combine to suggest that the level of attenuation in near-surface rocks (low pressures) is dominated by the increase in

Table 3

Mean results for the different intervals studied. All intervals are at the borehole except the one noted at the granite site. Errors are the standard deviation (S.D.) of the results from the different earthquakes. The results from fitting the mean spectral values are denoted $\overline{Q_P}$, $\overline{A_P}$, etc. The V_P/V_S ratio errors are (V_P + S.D.)/(V_S − S.D.) to (V_P − S.D.)/V_S + S.D.). Errors in V_P and V_S beneath the granite site (*) are estimated from the longest and shortest probable paths between the two recordings. The values below 2.5 km are from Abercrombie (1995a,b).

Depth Interval (km)	A_P (1 Hz)	$\overline{A_P}$ (1 Hz)	A_S (1 Hz)	$\overline{A_S}$ (1 Hz)	Q_P	$\overline{Q_P}$	Q_S	$\overline{Q_S}$	V_P (km/sec)	V_S (km/sec)	V_P/V_S	σ
0–25	12 ± 6	8.2	10 ± 3	9.5	27 ± 7	29	18 ± 4	22	5.39 ± 0.45	2.59 ± 0.21	2.08 ± 0.35	0.35
0–2.9 (granite)	1.2	—	3.6	—	50	—	23	—	6.1 ± 0.4*	3.2 ± 0.2*	1.9	0.31
0–2.9	13 ± 8.9	9.1	13 ± 11	7.0	27 ± 10	28	25 ± 10	31	4.42 ± 0.39	2.09 ± 0.35	2.11 ± 0.55	0.36
0–0.3	12 ± 8.9	8.7	22 ± 19	19	24 ± 14	26	17 ± 12	15	1.79 ± 0.05	0.657 ± 0.05	2.72 ± 0.24	0.42
0.3–1.5	1.3 ± 0.8	1.0	1.9 ± 0.8	1.6	36 ± 11	40	24 ± 6	25	4.63 ± 0.18	2.24 ± 0.13	2.07 ± 0.21	0.35
1.5–2.9	0.7 ± 0.2	0.56	1.1 ± 0.4	1.0	106 ± 80	133	52 ± 38	47	5.98 ± 0.16	3.42 ± 0.17	1.75 ± 0.2	0.26
>2.5					1000		1000		6.00	3.42	1.73	0.25

fracture content and probably other heterogeneities with decreasing overburden, and not simply the rock type.

At Cajon Pass, the ratios of Q_P to Q_S above 3 km are, on average, lower than the theoretical relationship for intrinsic attenuation in a dry, elastic, Poisson solid [$Q_P = (9/4)Q_S$, Knopoff, 1964]. The Earth, however, is not simply a dry solid but contains fluids. The Q_P/Q_S ratio has been found to vary with the degree of fluid saturation of the rock in a complex manner in laboratory studies (Winkler and Nur, 1979). Also, seismic waves are attenuated by scattering as well as intrinsic processes. The values obtained here are comparable with previous studies (Aster and Shearer, 1991; Blakeslee and Malin, 1991) but are not well enough constrained to investigate the fluid saturation of the rock column. This is true of previous borehole studies and also studies that use the spectral ratios between the direct S wave and the S-to-P conversion at the sediment–basement interface to determine Q_P/Q_S. For example, Clouser and Langston (1991) and Chen *et al.* (1994) find that Q_P/Q_S in sedimentary basins in Gazli and New Madrid, respectively, is strongly dependent on the unknown absolute values of Q_P and Q_S. In both studies, values similar to those obtained at Cajon Pass are consistent with their results.

Amplification in the near surface appears to be more site dependent than the associated attenuation. At the granite site, little amplification is observed; assuming that the free-surface effect is two, P waves experience negligible amplification and S waves less than a factor of 2. At the wellhead site, the amplification in the upper 2.5 to 3 km, averaged from phases I and II, is 13 ± 7 (1 standard deviation) for S waves and 12 ± 7 for P waves, with most of the amplification occurring at the surface and in the sedimentary layer. Using the values in Table 5, taken from the borehole logs (Vernik and Nur, 1992), the expected amplification can be estimated from the impedance contrast (Joyner *et al.*, 1981). The free-surface reflection is assumed to be two, as the surface incidence is approximately vertical. An average incidence angle at depth of 45° is taken from Table 1, and the densities and velocities are from Table 5. The borehole logs did not begin at the surface, and so the velocity and density values at the surface are maximum estimates. The expected P-wave amplification (including the effect of the free surface) in the upper 2.5 km is therefore ≧3.2 and the S-wave amplification ≧4. These values are rather smaller than those obtained from the spectral ratios. It is probable that the actual surface density and velocities are considerably lower than the estimates in Table 5. If they are similar to those found by Aster and Shearer (1991) in the top 5 m of weathered granite at Anza (density = 1.5 kg/m^3, V_P = 0.3 km/sec, and V_S = 0.3 km/sec), then the expected amplification in the upper 2.5 km would be about 10 for P waves and 9 for S waves. The amplification of the direct waves, obtained from the spectral ratios, thus appears to be in reasonable agreement with that expected from the impedance contrast. This is also true for the deeper intervals.

The inclusion of scattered energy following the direct wave in the surface seismograms (see Figs. 3c and 3d) could cause the spectral ratios to overestimate the amplification. This is minimized by using short time windows but cannot be excluded entirely. No clear arrivals are observed, following the direct waves, that can be related to any known interface in the rock column. Modeling the seismograms would be the logical step to improving our understanding of the near-surface amplification and attenuation and to investigating the source of scattered energy. The steep dip of the fault forming the sediment–basement contact in the borehole and the lack of information concerning the nature of slip, strike, and cumulative throw on this fault and the sediment depth to either side of it (Silver and James, 1988b; Pezard *et al.*, 1988) render simple one-dimensional modeling of wave propagation of limited value and two- and three-dimensional modeling unconstrained. The variation between events in amplification and Q is quite high, as might be expected from such a complex near-surface structure, but does not exhibit any clear azimuthal dependence. It should be noted that the inclusion of surface-recorded scattered energy

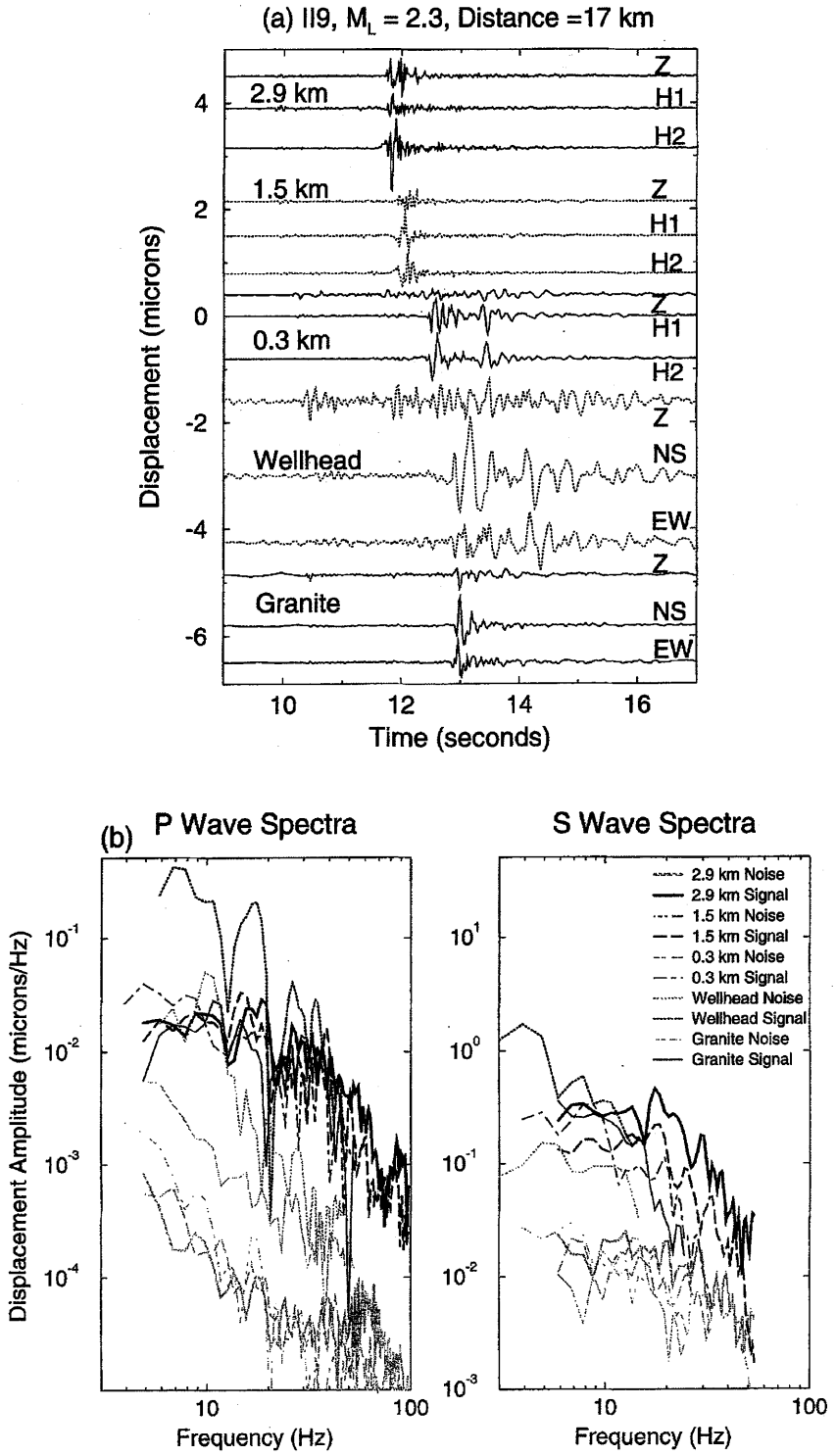

Figure 6. (a) seismograms and (b) spectra of event II9 recorded at four depths in the borehole and at the nearby granite site. All seismograms and spectra have been corrected for instrument response and are flat to displacement from 2 to 200 Hz. The noise spectra (gray) are from the pre-event noise for the *P* waves and the end of the *P*-wave coda for the *S* waves. Only the signal bandwidth used in the spectral ratios is shown.

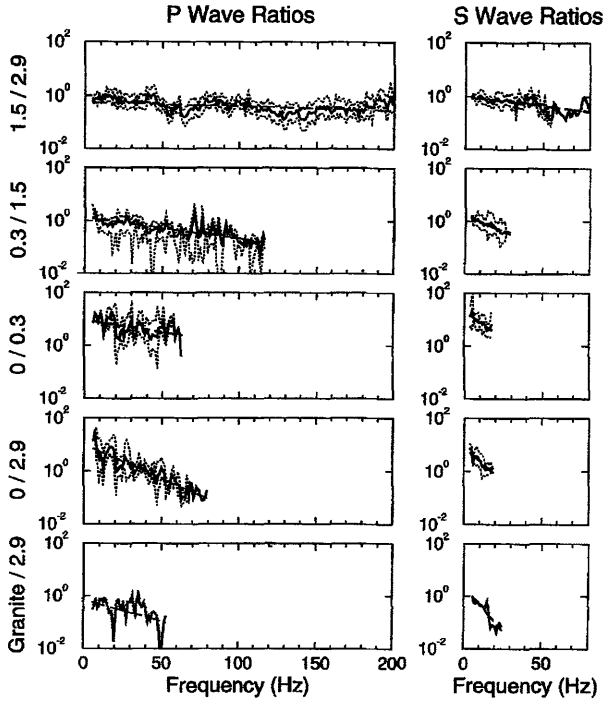

Figure 7. Mean *P*- and *S*-wave spectral ratios (solid lines) and best fits (dashed lines) using equation (1) for all phase II earthquakes recorded at the borehole. The spectral ratios between the granite site and 2.9 km are for event II9, the only earthquake recorded at both sites. Note that all 10 plots are at the same scale.

in the spectral ratios will also affect the Q values obtained. This is because the time traveled by the scattered energy is larger than that of the direct waves, and so if a significant amount of scattered energy is included, the Q values obtained would be underestimates. This is more likely to be a problem for the *P* waves than the *S* waves as the length of the time window used is longer with respect to the interval travel times of the direct *P* waves than the slower *S* waves. Calculations considering average travel times, and the fact that the seismograms used are all impulsive, suggest that this would have a small effect, well within the error bars quoted in Table 3. Also, this problem is common to all such spectral ratio studies and is minimized here by the relatively short time windows used.

The use of coda waves has become common for estimating site response and amplification (e.g., Phillips and Aki, 1986; Mayeda *et al.*, 1991; Su *et al.*, 1992), and so this method is also considered here for comparison with the direct-wave results. The amplitude spectra of a 0.5-sec moving window are calculated for the seismograms of event II9, the only event recorded at the granite site. The windows start at the time of the *S*-wave arrival and continue as far into the coda as there is good signal to noise at the 2.9-km, wellhead, and granite sites. The average amplitude of the ratios of the two surface sites to the 2.9-km site are then measured between 6 and 8 Hz. The signal is too small at the surface to consider coda amplification at higher frequencies. The results are plotted in Figure 8. After about 2 sec, the amplitude at the granite site has returned to the level calculated for the direct wave. The coda-wave amplification at the sedimentary (wellhead) site is three times higher than the direct wave even after twice the *S*-wave travel time and shows no sign of returning to the direct-wave ratio. These results are similar to those of Margheriti *et al.* (1994) and Field (1995) who find that in sedimentary basins, scattered energy leads to increased coda-wave amplification factors at several times the *S*-wave travel time. Su *et al.* (1996) compare direct-*S*-wave and coda-wave site amplification for a range of earthquakes and stations in the frequency range 0.5 to 30 Hz. They find that the two amplification factors are comparable for epicentral distances greater than 10 km, but exhibit some variation for closer events. On the basis of these observations, they suggest that the amplification of the direct *S* waves may be affected by the particular propagation path for small epicentral distances. This suggestion is consistent with the variation in measured parameters for the individual earthquakes considered in this study. It is also worth noting, however, that Su *et al.* (1996) use 5-sec time windows for both direct and coda waves, considerably longer than required by the corner frequencies of the earthquakes they use (approximately 3 Hz, Abercrombie, 1995a). They, therefore, include considerable scattered energy in the direct-*S*-wave windows (cf. Figs. 6a and 8) and so may overestimate the direct *S*-wave amplification factors. Where scattered phases

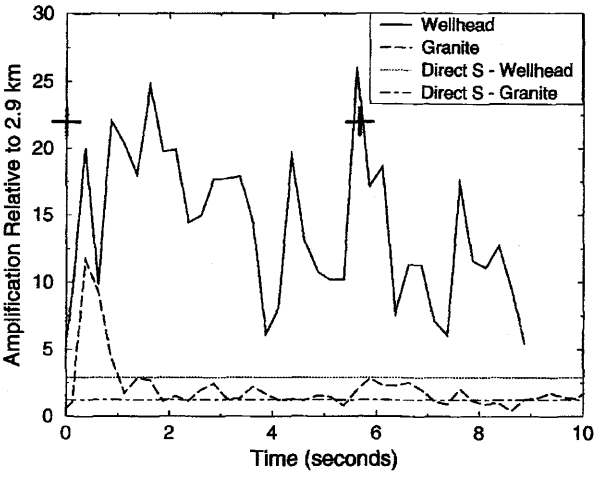

Figure 8. Comparison of coda- and direct-wave estimates of mean amplification between 6 and 8 Hz for event II9. The dotted and dot-dashed lines mark the amplification calculated for the direct waves at 7 Hz. The solid and dashed lines represent the amplification in a moving window into the coda. The two plus signs mark one and two times the *S*-wave travel time to the most distant station, measured from the earthquake origin time.

Table 4
A selection of near-surface attenuation results in borehole (≥100 m) studies in California.

Location	Depth Range (m)	Q_P	Q_S	Rock Type	Authors
Oroville	0–475	—	9	ophiolite	Malin *et al.* (1988)
Oroville	375–475	—	11	ophiolite	Malin *et al.* (1988)
Anza	0–150	6.5	9	granite	Aster and Shearer (1991)
Anza	150–300	27	26	granite	Aster and Shearer (1991)
Garner Valley	0–220	—	12	soil, weathered granite, and granite	Archuleta *et al.* (1992)
Santa Clara Valley	10–35	—	10	Quaternary alluvium	Gibbs *et al.* (1994)
Santa Clara Valley	40–115	—	15	Quaternary alluvium	Gibbs *et al.* (1994)
Parkfield	0–200	6–11	8–19	Tertiary sediments	Blakeslee and Malin (1991)
Parkfield	0–300	—	10	Tertiary sediments	Jongmans and Malin (1995)
Parkfield	0–1000	—	37	Tertiary sediments	Jongmans and Malin (1995)
Los Angeles basin	0–420	45	—	Pleistocene and Pliocene sediments	Hauksson *et al.* (1987)
Los Angeles basin	420–1500	43	25	Pleistocene and Pliocene sediments	Hauksson *et al.* (1987)

Table 5
Materials properties from the logs of the Cajon Pass drillhole. The logs did not begin at the surface, and so the surface values (*) are estimated from the density at 50 m (from the log) and the average velocities in the upper 300 m in Table 3.

Depth (km)	Density (kg/m^3)	V_P (km/sec)	V_S (km/sec)
0	≦2.4*	≦1.8*	≦0.66*
0.3	2.54	3.3	—
1.5	2.69	5.4	3.0
2.5	2.71	5.7	3.3
2.9	2.75	6.0	3.5

are the largest in the seismogram, the coda-wave amplification factors are valid for seismic hazard investigations. Care should be taken, however, in using coda-wave amplification factors to estimate the amplification of the direct waves as this could result in significant overestimation at sedimentary sites.

Comparison of arrival times of the earthquakes at the different levels allows a good estimate of the velocities of both the P and S waves to be calculated. Both are seen to decrease toward the surface as expected, and the results obtained here for P waves are in good agreement with the borehole sonic log (Table 5, Vernik and Nur, 1992) and VSP studies in the Cajon Pass hole (Li *et al.*, 1988). Of more interest is the increase in V_P/V_S and Poisson's ratio (σ) to about 2.1 ($\sigma = 0.36$) for the whole 3 km and 2.7 ($\sigma = 0.42$) in the upper 300 m, respectively. At the granite site, the increases are smaller but still significant ($V_P/V_S = 1.9, \sigma = 0.31$ in the upper 3 km). Such increases are observed in exploration studies that use both P and S waves and also in borehole sonic logs (e.g., Vernik and Nur, 1992; Moos and Zoback, 1983). Increases in V_P/V_S are not commonly included in site-effect studies or in inversions for crustal velocity structure and earthquake locations. Nicholson and Simpson (1985) find that allowing V_P/V_S to increase at shallow depths improves the stability of earthquake hypocenter determination and increases the resolution of shallow seismicity patterns.

Conclusions

1. Near-surface attenuation is significant with $Q_P \sim 27 \pm 8$ at the borehole site and ~50 at a nearby granite site, averaged over the upper 3 km, and measured between 5 and 100 Hz; $Q_S \sim 21 \pm 7$ at both sites. Compared with $Q \sim 1000$ below 3 km (Abercrombie, 1995a), at least 90% of attenuation of an earthquake within 15 km of the borehole occurs in the upper 3 km. Also, near-surface attenuation appears less dependent on rock type than does the amplification.
2. The amplification (including the free-surface effect) of the direct P and S waves in the upper 3 km at the wellhead (about 12 ± 7 and 13 ± 7, respectively, at 1 Hz) is in reasonable agreement with that predicted by the impedance contrast and the free-surface effect. Near-surface amplification is less than two for P waves and less than four for S waves at the granite site; amplification at the wellhead is therefore more than three times higher at the wellhead than at the granite site.
3. Coda-wave amplification estimates at twice the S-wave travel time are comparable to the direct-wave amplification factors at the granite site but at least three times higher at the wellhead. Coda-wave amplification factors should, therefore, not be used to predict the amplification of the direct waves.

Acknowledgments

I am grateful to P. Leary and D. Manov for invaluable assistance with the installation of the deep borehole seismometers, to M. Robertson, A. Martin, L. Fields, and M. Ragan for help with the data recording, and to L. Teng, P. Davis, the California Department of Mines and Geology, the Southern California Earthquake Center (SCEC), and IRIS (PASSCAL) for generously loaning RefTek recording equipment. P. Passmore and D. Pavel

(RefTek) generously designed and gave us an optically isolated triggering box, enabling us to connect the three RefTeks together in phase II. I also thank E. Field for helpful discussions and reviews of early versions of this manuscript. J. Steidl, R. Archuleta, M. Fehler, R. Benites, D. Boore, and an anonymous reviewer provided helpful comments that improved this article. The borehole seismometers were installed under NSF awards EAR-9004381 and EAR-9219856, and REA was also supported in part by SCEC. This is SCEC Contribution Number 207.

References

Abercrombie, R. E. (1995a). Earthquake source scaling relationships from -1 to 5 M_L using seismograms recorded at 2.5 km depth, *J. Geophys. Res.* **100,** 24015–24036.

Abercrombie, R. E. (1995b). Earthquake locations using single-station deep borehole recordings: implications for microseismicity on the San Andreas fault in sourthern California, *J. Geophys. Res.* **100,** 24003–24014.

Abercrombie, R. E. and P. Leary (1993). Source parameters of small earthquakes recorded at 2.5 km depth, Cajon Pass, southern California: implications for earthquake scaling, *Geophys. Res. Lett.* **20,** 1511–1514.

Anderson, J. G. (1986). Implication of attenuation for studies of the earthquake source, in *Earthquake Source Mechanics,* S. Das, J. Boatwright, and C. H. Scholz (Editors), American Geophysical Monograph 37, 311–318.

Archuleta, R. J., E. Cranswick, C. Mueller, and P. Spudich (1982). Source parameters of the 1980 Mammoth Lakes, California, earthquake sequence, *J. Geophys. Res.* **87,** 4595–4607.

Archuleta, R. J., S. H. Seale, P. V. Sangas, L. M. Baker, and S. T. Swain (1992). Garner Valley downhole array of accelerometers: instrumentation and preliminary data analysis, *Bull. Seism. Soc. Am.* **82,** 1592–1621.

Aster, R. C. and P. M. Shearer (1991). High-frequency borehole seismograms recorded in the San Jacinto fault zone, southern California: Part 2. Attenuation and site effects, *Bull. Seism. Soc. Am.* **81,** 1081–1100.

Blakeslee, S. and P. Malin (1991). High-frequency site effects at two Parkfield downhole and surface stations, *Bull. Seism. Soc. Am.* **81,** 332–345.

Borcherdt, R. D. (1970). The effects of local geology on ground motion near San Francisco Bay, *Bull. Seism. Soc. Am.* **60,** 29–61.

Celebi, M., J. Prince, C. Dietal, M. Onate, and G. Chavez (1987). The culprit in Mexico City—amplification of motions, *Earthquake Spectra* **3,** 315–328.

Chen, K.-C., J.-M. Chiu, and Y.-T. Yang (1994). Q_P-Q_S relations in the sedimentary basin of the Upper Mississippi embayment using converted phases, *Bull. Seism. Soc. Am.* **84,** 1861–1868.

Clouser, R. H. and C. A. Langston (1991). Q_P-Q_S relations in a sedimentary basin using converted phases, *Bull. Seism. Soc. Am.* **81,** 733–750.

Field, E. H. (1995). Site response estimates in the Coachella valley, *Seism. Res. Lett.* **66,** 31.

Field, E. H., K. H. Jacob, and S. H. Hough (1992). Earthquake site response estimation: a weak-motion case study, *Bull. Seism. Soc. Am.* **82,** 2283–2307.

Field, E. H. and K. H. Jacob (1995). A comparison and test of various site response estimation techniques, including three that are non reference site dependent, *Bull. Seism. Soc. Am.* **85,** 1127–1143.

Frankel, A. and L. Wennerberg (1989). Microearthquake spectra from the Anza, California, seismic network: site response and source scaling, *Bull. Seism. Soc. Am.* **79,** 581–609.

Gibbs, J. F., D. M. Boore, W. B. Joyner, and T. E. Fumal (1994). The attenuation of seismic shear waves in Quaternary alluvium in Santa Clara valley, California, *Bull. Seism. Soc. Am.* **84,** 76–90.

Hauksson, E., T.-L. Teng, and T. L. Henyey (1987). Results from a 1500 m deep, three-level downhole seismometer array: site response, low Q values and f_{max}, *Bull. Seism. Soc. Am.* **77,** 1883–1904.

Jin, A., K. Mayeda, D. Adams, and K. Aki (1994). Separation of intrinsic and scattering attenuation in southern California using TERRAscope data, *J. Geophys. Res.* **99,** 17835–17848.

Johnston, D. H., M. N. Toksoz, and A. Timur (1979). Attenuation of seismic waves in dry and saturated rocks: II. Mechanisms, *Geophysics* **44,** 691–711.

Jongmans, D. and P. E. Malin (1995). Vertical profiling of microearthquake S waves in the Varian well at Parkfield, California, *Bull. Seism. Soc. Am.* **85,** 1805–1820.

Joyner, W. B., R. E. Warrick, and T. E. Fumal (1981). The effect of Quaternary alluvium on strong ground motion in the Coyote Lake, California, earthquake of 1979, *Bull. Seism. Soc. Am.* **71,** 1333–1349.

Knopoff, L. (1964). *Q, Rev. Geophys.* **2,** 625–660.

Leary, P. C. and R. E. Abercrombie (1994). Frequency dependent crustal scattering and absorption at 5–160 Hz from coda decay observed at 2.5 km depth, *Geophys. Res. Lett.* **21,** 971–974.

Leary, P. C., Y.-G. Li, and D. V. Manov (1990). A microprocessor-based borehole seismic sonde, *Bull. Seism. Soc. Am.* **80,** 717–736.

Li, Y.-G., P. C. Leary, and T. L. Henyey (1988). Stress orientation inferred from shear wave splitting in basement rock at Cajon Pass, *Geophys. Res. Lett.* **15,** 997–1000.

Magistrale, H., H. Kanamori, and C. Jones (1992). Forward and inverse three-dimensional P wave velocity models of the Southern California crust, *J. Geophys. Res.,* **97,** 14115–14135.

Malin, P. E., J. A. Waller, R. D. Borcherdt, E. Cranswick, E. G. Jensen, and J. Van Schaack (1988). Vertical seismic profiling of Oroville microearthquakes: velocity spectra and particle motion as a function of depth, *Bull. Seism. Soc. Am.* **78,** 401–420.

Manov, D. V., R. E. Abercrombie, and P. C. Leary (1996). Reliable and economical high temperature deep borehole seismic recording, *Bull. Seism. Soc. Am.* **86,** 204–211.

Margheriti, L., L. Wennerberg, and J. Boatwright (1994). A comparison of coda and S wave spectral ratios as estimates of site response in the southern San Francisco Bay area, *Bull. Seism. Soc. Am.* **84,** 1815–1830.

Mayeda, K., S. Koyanagi, and K. Aki (1991). Site amplification from S wave coda in the Long Valley caldera region, California, *Bull. Seism. Soc. Am.* **81,** 2194–2213.

Meisling, K. E. and R. J. Weldon (1989). Late Cenozoic tectonics of the northwestern San Bernardino Mountains, southern California, *Geol. Soc. Am. Bull.* **101,** 106–128.

Moos, D. and M. D. Zoback (1983). In situ studies of seismic velocity in fractured crystalline rocks, *J. Geophys. Res.* **88,** 2345–2358.

Mori, J. and A. Frankel (1991). Depth dependent scattering shown by coherence estimates and regional coda amplitudes, *EOS (Supplement)* **72,** 344.

Nicholson, C. and D. W. Simpson (1985). Changes in V_P/V_S with depth: implications for appropriate velocity models, improved earthquake locations, and material properties of the upper crust, *Bull. Seism. Soc. Am.* **75,** 1105–1123.

Pezard, P. A., R. J. Weldon, R. N. Anderson, C. R. Wilkinson, and G. R. Ollier (1988). Constraints on the geometries of structures within the sedimentary rocks at the Cajon Pass scientific drillsite, California, *Geophys. Res. Lett.,* **15,** 965–968.

Phillips, W. S. and K. Aki (1986). Site amplification of coda waves from local earthquakes in central California, *Bull. Seism. Soc. Am.* **76,** 627–648.

Rodgers, P. W., A. J. Martin, M. C. Robertson, M. M. Hsu, and D. B. Harris (1995). Signal-coil calibration of electromagnetic seismometers, *Bull. Seism. Soc. Am.* **85,** 845–850.

Seale, S. H. and R. J. Archuleta (1989). Site amplification and attenuation of strong ground motion, *Bull. Seism. Soc. Am.* **79,** 1673–1696.

Shearer, P. M. and J. A. Orcutt (1987). Surface and near-surface effects on seismic waves—theory and borehole seismometer results, *Bull. Seism. Soc. Am.* **77,** 1168–1196.

Silver, L. T. and E. W. James (1988a). Lithologic column of the "Arkoma"

drillhole and its relation to the Cajon Pass deep drillhole, *Geophys. Res. Lett.* **15,** 945–948.

Silver, L. T. and E. W. James (1988b). Geologic setting and lithologic column of the Cajon Pass deep drillhole, *Geophys. Res. Lett.* **15,** 941–944.

Su, F., K. Aki, T. Teng, S. Koyanagi, and K. Mayeda (1992). The relation between site amplification factor and surficial geology in central California, *Bull. Seism. Soc. Am.* **82,** 580–602.

Su, F., J. G. Anderson, J. N. Brune, and Y. Zeng (1996). A comparison of direct S-wave and coda-wave site amplification determined from aftershocks of the Little Skull Mountain earthquake, *Bull. Seism. Soc. Am.* **86,** 1006–1018.

Vernik, L. and A. Nur (1992). Petrophysical analysis of the Cajon Pass scientific well: implications for fluid flow and seismic studies in the continental crust, *J. Geophys. Res.* **97,** 5121–5134.

Winkler, K. and A. Nur (1979). Pore fluids and seismic attenuation in rocks, *Geophys. Res. Lett.* **6,** 1–4.

Yerkes, R. F., T. H. McCulloch, J. G. Schoellhamer, and J. G. Vedder (1965). Geology of the Los Angeles Basin, California—an introduction, *U.S. Geol. Surv. Profess. Pap. 420-A.*

Zeng, Z. and J. G. Anderson (1996). A composite source model of the 1994 Northridge earthquake using genetic algorithms, *Bull. Seism. Soc. Am.* **86,** S71–S83.

Department of Earth Sciences
University of Southern California
Los Angeles, California 90089

Manuscript received 3 July 1995.